

# The COMBLE Campaign

## A Study of Marine Boundary Layer Clouds in Arctic Cold-Air Outbreaks

Bart Geerts, Scott E. Giangrande, Greg M. McFarquhar, Lulin Xue, Steven J. Abel, Jennifer M. Comstock, Susanne Crewell, Paul J. DeMott, Kerstin Ebell, Paul Field, Thomas C. J. Hill, Alexis Hunzinger, Michael P. Jensen, Karen L. Johnson, Timothy W. Juliano, Pavlos Kollias, Branko Kosovic, Christian Lackner, Ed Luke, Christof Lüpkes, Alyssa A. Matthews, Roel Neggers, Mikhail Ovchinnikov, Heath Powers, Matthew D. Shupe, Thomas Spengler, Benjamin E. Swanson, Michael Tjernström, Adam K. Theisen, Nathan A. Wales, Yonggang Wang, Manfred Wendisch, and Peng Wu

**ABSTRACT:** One of the most intense air mass transformations on Earth happens when cold air flows from frozen surfaces to much warmer open water in cold-air outbreaks (CAOs), a process captured beautifully in satellite imagery. Despite the ubiquity of the CAO cloud regime over high-latitude oceans, we have a rather poor understanding of its properties, its role in energy and water cycles, and its treatment in weather and climate models. The Cold-Air Outbreaks in the Marine Boundary Layer Experiment (COMBLE) was conducted to better understand this regime and its representation in models. COMBLE aimed to examine the relations between surface fluxes, boundary layer structure, aerosol, cloud, and precipitation properties, and mesoscale circulations in marine CAOs. Processes affecting these properties largely fall in a range of scales where boundary layer processes, convection, and precipitation are tightly coupled, which makes accurate representation of the CAO cloud regime in numerical weather prediction and global climate models most challenging. COMBLE deployed an Atmospheric Radiation Measurement Mobile Facility at a coastal site in northern Scandinavia (69°N), with additional instruments on Bear Island (75°N), from December 2019 to May 2020. CAO conditions were experienced 19% (21%) of the time at the main site (on Bear Island). A comprehensive suite of continuous in situ and remote sensing observations of atmospheric conditions, clouds, precipitation, and aerosol were collected. Because of the clouds' well-defined origin, their shallow depth, and the broad range of observed temperature and aerosol concentrations, the COMBLE dataset provides a powerful modeling testbed for improving the representation of mixed-phase cloud processes in large-eddy simulations and large-scale models.

**KEYWORDS:** Arctic; Cold air surges; Marine boundary layer; Cloud water/phase; Cloud resolving models; Aerosol-cloud interaction

<https://doi.org/10.1175/BAMS-D-21-0044.1>

Corresponding author: Bart Geerts, [geerts@uwyo.edu](mailto:geerts@uwyo.edu)

Supplemental material: <https://doi.org/10.1175/BAMS-D-21-0044.2>

In final form 13 February 2022

©2022 American Meteorological Society

For information regarding reuse of this content and general copyright information, consult the [AMS Copyright Policy](#).

**AFFILIATIONS:** **Geerts and Lackner**—University of Wyoming, Laramie, Wyoming; **Giangrande, Jensen, Johnson, and Luke**—Brookhaven National Laboratory, Upton, New York; **McFarquhar**—University of Oklahoma, Norman, Oklahoma; **Xue, Juliano, and Kosovic**—National Center for Atmospheric Research, Boulder, Colorado; **Abel and Field**—Met Office, Exeter, United Kingdom; **Comstock, Matthews, Ovchinnikov, and Wu**—Pacific Northwest National Laboratory, Richland, Washington; **Crewell, Ebell, and Neggens**—University of Cologne, Cologne, Germany; **DeMott, Hill, and Swanson**—Colorado State University, Fort Collins, Colorado; **Hunzinger**—NASA Goddard, Greenbelt, Maryland; **Kollias**—Stony Brook University, Stony Brook, and Brookhaven National Laboratory, Upton, New York; **Lüpkes**—Alfred Wegener Institute, Bremerhaven, Germany; **Powers and Wales**—Los Alamos National Laboratory, Los Alamos, New Mexico; **Shupe**—University of Colorado Boulder, and NOAA Physical Sciences Laboratory, Boulder, Colorado; **Spengler**—University of Bergen, Bergen, Norway; **Tjernström**—Stockholm University, Stockholm, Sweden; **Theisen**—Argonne National Laboratory, Lemont, Illinois; **Wang**—State University of New York at Oswego, Oswego, New York; **Wendisch**—University of Leipzig, Leipzig, Germany

One of the main uncertainties of climate models is the response of clouds to global warming (IPCC 2021). Consider, hypothetically, a field of mixed-phase clouds (containing both supercooled liquid water and ice particles) over an ocean: all else being equal, will the ice fraction be reduced in these clouds as the surface temperature rises? Will this reduce the rate and frequency of precipitation? Will this increase the albedo of this cloud regime, given that a cloud with numerous cloud droplets is brighter than an ice-dominated cloud, and given that the delay in precipitation may increase the cloud's lifespan and the overall cloud fraction? Affirmative answers to these process questions imply a negative feedback, as the higher albedo would counter the warming (e.g., McCoy et al. 2014). Reducing cloud-related uncertainties requires evaluation and improvement of not only climate models, but also the cloud-resolving, large-eddy simulations (LES) and other models that are used to develop and test parameterizations of physical processes in climate models (e.g., de Roode et al. 2019). Any advancement in climate models and their LES building blocks requires an understanding and accurate representation of the physical processes that ultimately depend on targeted and well-calibrated observations.

One particular synoptic regime where model improvement (and thus targeted observations) is needed is the cold-air outbreak (CAO) cloud regime. This regime consists of shallow convective clouds that form when cold continental or polar air masses are advected over open water. Satellite and radar imagery (Fig. 1) show how the mesoscale cloud and precipitation structure of this regime evolves as the boundary layer (BL) deepens with increasing fetch in response to surface heat fluxes, from a few hundred meters near the ice edge to ~4 km near the Scandinavian coast in this case. In general, a linear arrangement of convective clouds ("streets"), whose width and spacing increases with BL depth, transitions at some fetch from the upstream edge of the open water to an open-cellular structure with cells of increasing size and spacing (e.g., Brümmner 1999). The BL clouds and associated circulations are the result of surface heat and moisture fluxes, large-scale subsidence (which prevails in CAOs) countered by entrainment across the BL top, as well as aerosol particle properties and radiative fluxes. Whereas the cloud streets reflect a series of horizontal convective rolls (HCRs) driven by shear in a BL heated from below (e.g., Young et al. 2002), there is increasing evidence that cloud processes play an essential role in the transition to an open-cellular structure (e.g., Tornow et al. 2021). CAO clouds represent a significant challenge to numerical weather prediction

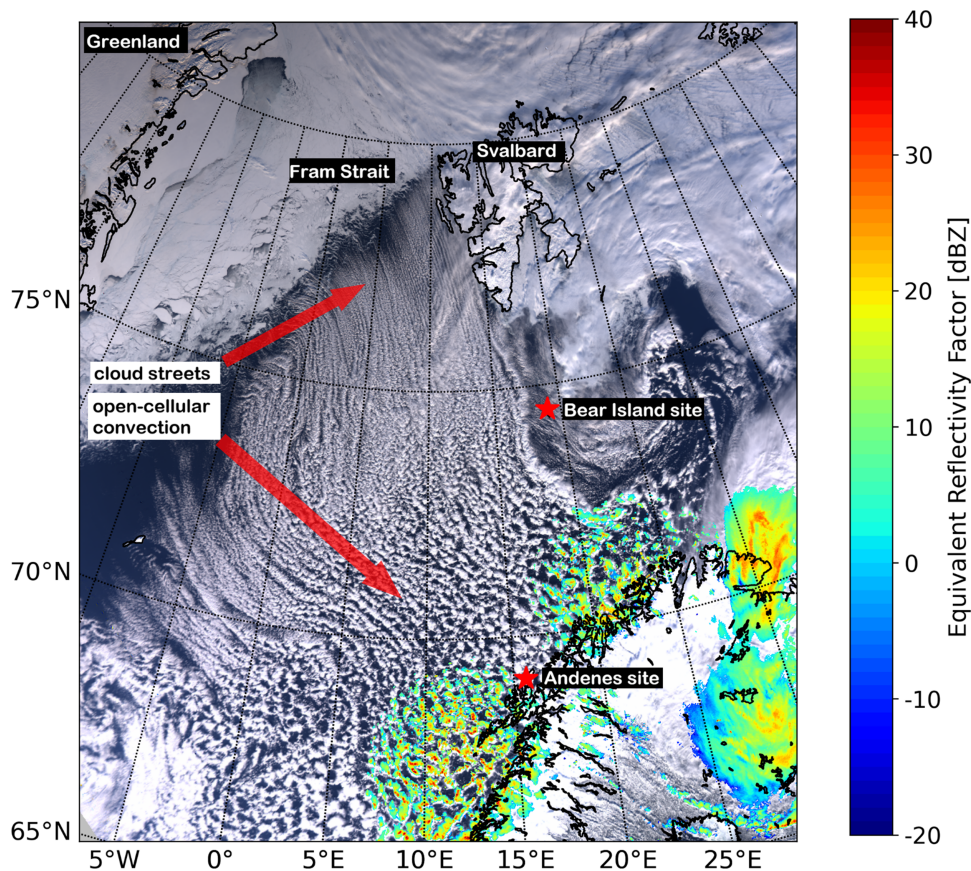


Fig. 1. MODIS visible image and radar reflectivity mosaic (with coverage over/near Scandinavia only) at 1040 UTC 28 Mar 2020. The radar mosaic is from the operational C-band radar network in Scandinavia.

(NWP) and climate models because CAO clouds fall in a dynamic “gray zone” where unresolved BL processes and moist convection cannot be parameterized independently (Field et al. 2017; Frassoni et al. 2018).

CAOs contribute substantially to the total air–sea heat exchange in climate-critical regions such as the far northern Atlantic (Papritz and Spengler 2017), thereby playing a key role in the formation of dense waters feeding into the lower limb of the Atlantic meridional overturning circulation (Dickson et al. 1996). The overall role of CAOs in the climate system is, however, still poorly understood. A key question related to the observed amplified Arctic climate change (Pithan and Mauritsen 2014) regards the dynamic exchange between the Arctic and the midlatitude belt, including possible cloud feedbacks (Vavrus 2004; Pithan et al. 2018). Climate models poorly capture marine BL clouds in CAOs (e.g., Field et al. 2014; Abel et al. 2017) and in the postfrontal cold sector in general (e.g., Naud et al. 2019). Satellite retrievals of cloud properties, such as from MODIS, *CloudSat*, and *CALIPSO*, are challenged in the CAO cloud regime by the small-scale heterogeneity of cloud properties (e.g., Fletcher et al. 2016; Ahn et al. 2018; Marchant et al. 2020). Little is known about the concentrations and budgets of cloud-active aerosol particles, the cloud phase distribution, the size distribution of liquid and snow particles and associated precipitation development processes, the range of surface precipitation rates, and the mechanisms that control cloud-dynamical transitions (McCoy et al. 2017).

To build the observational database needed to improve our understanding of these CAO processes, the U.S. Department of Energy (DOE) deployed the first Atmospheric Radiation Measurement (ARM) Mobile Facility (AMF) (Mather and Voyles 2013; Miller et al. 2016) at a coastal site near Andenes in northern Scandinavia (69°N, 16°E), located 1,000–1,300 km from

the Arctic ice edge (Fig. 2), from 1 December 2019 to 31 May 2020. As part of this field campaign, referred to as Cold-Air Outbreaks in the Marine Boundary Layer Experiment (COMBLE), a number of in situ and remote atmospheric sensors were also deployed on Bjørnøya (or Bear Island, 75°N, 19°E) in the Norwegian Sea. COMBLE overlapped with the Ny-Ålesund Aerosol Cloud Experiment (NASCENT), conducted in 2019–20 at several atmospheric observatories in Ny-Ålesund on Svalbard (Pasquier et al. 2021, manuscript submitted to *Bull. Amer. Meteor. Soc.*), and the Multidisciplinary Observatory for the Study of Arctic Climate (MOSAIC) expedition aboard the icebreaker *Polarstern* drifting in the Arctic sea ice (Shupe et al. 2022) (Fig. 2).

## Objectives

The COMBLE campaign sampled the marine CAO regime in a range of upstream wind, temperature, and stability conditions. Three specific objectives are pursued with the COMBLE dataset. First, we seek process-level understanding, through the description of the mesoscale organization of airflow, clouds, and precipitation, combined with the vertical structure of temperature, humidity, vertical velocity, turbulent kinetic energy, and cloud and precipitation properties within and between convective elements.

Second, we examine how varying aerosol conditions in the upstream Arctic lower and middle troposphere (possibly transported over long distances and mixed down into the convective BL), as well as marine aerosol sources, impact ice initiation, cloud liquid water, snow growth, and radiative fluxes.

And third, we aim to use the integrated COMBLE datasets of dynamical, thermodynamic, and microphysical characteristics of the marine BL, including cloud and aerosol properties, to

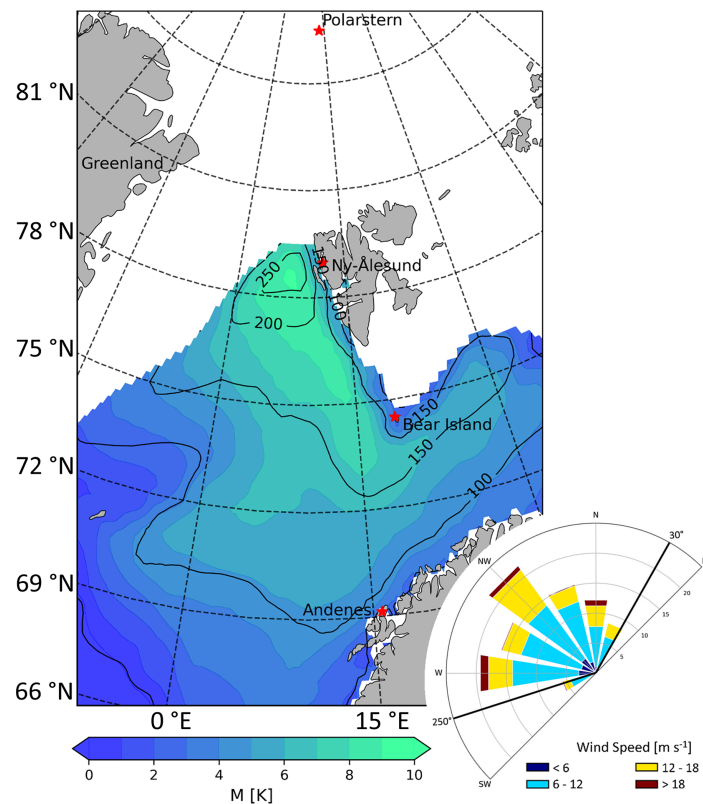


Fig. 2. Map of average surface sensible heat fluxes (contoured;  $\text{W m}^{-2}$ ), and ice edge location (white areas have  $>50\%$  ice fraction) during CAO conditions at Andenes during COMBLE (1 Dec 2019–31 May 2020) (source: ECMWF Reanalysis v5, or ERA5). The color field is  $M \equiv \theta_{\text{SST}} - \theta_{850\text{hPa}}$ , a measure of thermal instability driven by surface heat fluxes. Also shown are the two COMBLE sites, the research site Ny-Ålesund on Svalbard, and the location of the *Polarstern* on 28 Mar 2020. The insert in the lower right is the Andenes wind rose (wind speed;  $\text{m s}^{-1}$ ) during CAO conditions during COMBLE.

evaluate and constrain high-resolution numerical simulations, and subsequently, to evaluate and improve representations of shallow convection in CAOs in NWP and climate models, and to examine the response of this cloud regime to warming climate. The well-defined upstream cloud boundary serves as an excellent testbed for aerosol–cloud–precipitation modeling studies, including secondary ice production.

These three objectives are not independent: the development of process-level understanding of shallow convective clouds in CAOs requires both observations and the dynamically and microphysically consistent output from models.

### The COMBLE field campaign

**Field operations.** The COMBLE campaign was highly successful, notwithstanding a number of challenges, including a rapid deployment less than 6 months after completion of another AMF1 deployment in the Southern Hemisphere, the darkness of the polar night, the inaccessibility of Bear Island (an uninhabited island some 500 km north of the Scandinavian mainland), the adverse weather conditions and instrument damage by polar bears on Bear Island, and the outbreak of a pandemic in the middle of the campaign. All instruments at the two sites (Fig. 3) were operational 1 month ahead of schedule (by 1 December 2019), increasing the sampling period by 20% compared to the requested deployment period (with a start date of 1 January 2020). COMBLE started off during the polar night; the sun first rose over the horizon at the Andenes site on 12 January and at the Bear Island site on 4 February 2020.

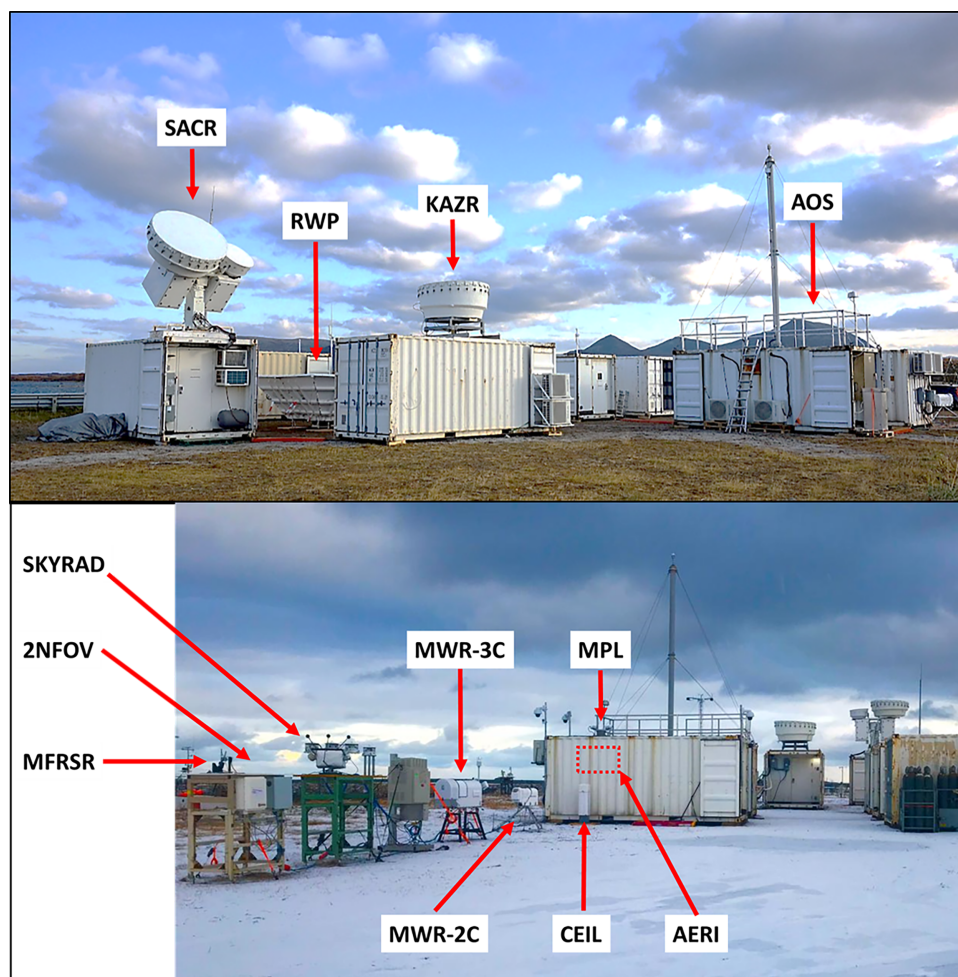


Fig. 3. Instruments at the AMF1, located on Andøya, an island just off the northern Norwegian mainland. The AMF1 was deployed at Nordmela harbor, which juts out slightly from the natural coastline. The top (bottom) image is looking to the south-southeast (north-northeast). Acronyms are defined in the appendix.

The success can be attributed at least in part to the ARM program's early decision to work closely with local resources, in particular with the Norwegian Meteorological Service (Met Norway). Met Norway personnel coordinated the installation and operation of ARM equipment and associated communication system on Bear Island, where it operates a manned weather station including 12-hourly WMO radiosondes. In collaboration with Met Norway, the Norwegian Coast Guard delivered the equipment to the island, where it had to be transferred via dinghy from the ship to the beach. Met Norway personnel launched radiosondes every three hours during CAOs, following a principal investigator (PI)-led forecasting procedure. The pandemic resulted in the cancellation of several separately funded airborne campaigns, with flights planned over or near the Andenes site in March–April 2020. The pandemic was disruptive to COMBLE operations as well, but measurements continued unabated through the scheduled end date of 31 May. This was accomplished notwithstanding Norway's lockdown, and was only possible through intensive diplomatic efforts (which allowed DOE personnel to secure approvals for exceptional travel), and through engagement with the local community and businesses. For instance, facing a personnel shortage at Andenes, local fishermen volunteered to help clear the snow and to assist with weather balloon launches.

Table 1 lists the instruments deployed at both sites, as well as derived meteorological quantities. The instruments, the data processing, and the value-added products are described in the online supplemental material. Offshore radar coverage was excellent at Andenes: in addition to the ARM W- and Ka-band scanning radars, there was an operational volume-scanning Met Norway C-band Doppler polarization radar (Trolltinde) close to the AMF1 site, on a ~300-m-high hill (Saltikoff et al. 2017). A profiling radar was deployed on Bear Island, but no scanning radar, so cloud morphology information around Bear Island can only be inferred from (infrequent) overpasses of the *Aqua*, *Terra*, and Visible Infrared Imaging Radiometer Suite (VIIRS) satellites.

**Survey of environmental conditions and cloud characteristics.** A cumulative total of 34 days of CAO conditions was observed at the AMF1 site during the 6-month COMBLE campaign. We define CAO conditions based on ambient wind and low-level static stability, as follows:  $M > 0$ , surface wind speed  $> 10$  kt (1 kt  $\approx 0.51$  m s<sup>-1</sup>), and, for a coastal site such as Andenes, surface wind direction onshore (in this case between 250° and 30°, shown as bold lines in Fig. 2). Here,  $M$  is defined as  $M \equiv \theta_{\text{SST}} - \theta_{850\text{hPa}}$ , where  $\theta$  is potential temperature and SST is the sea surface temperature just offshore Andoya. It is a commonly used index of thermal instability driven by heat fluxes from the underlying water surface (e.g., Papritz et al. 2015). Based on this definition, the average  $M$  value during all CAOs at Andenes during COMBLE was 4.1 K (Fig. 4), with higher values closer to the ice edge, in the Fram Strait (Fig. 2). This pattern is consistent with a 10-yr ERA5-based climatology (not shown). In other words, CAOs are synoptic events and the cloud structures sampled at Andenes are the result of surface, BL, and microphysical processes over a distance of  $O(1,000)$  km, or 1–2 days under typical winds. Such dependence on upstream conditions becomes even more evident in a Lagrangian CAO climatology (Papritz and Spengler 2017).

A wide range of CAO intensities was observed at Andenes, with 10th (90th) percentile  $M$  values of 1.3 K (7.1 K), resulting in very different cloud depths and structures. Cloud depths were generally below 2 km; a small fraction of the cloud depths exceeded 4 km (Fig. 4f). Cloud depth is defined as the local KAZR echo-top height minus the ceilometer base height. Because of the relatively high sea surface temperature (SST) off Andenes, the cloud base was usually rather high during onshore flow (0.4–1.0 km). The CAO clouds often contained much liquid, usually associated with early convective development. Approximately 12% of the cloud profiles had liquid water path (LWP) values exceeding 500 g m<sup>-2</sup> (Fig. 4c).

**Table 1. Instruments, primary measurements, derived quantities.**

Instrument	Primary measurement	Derived quantities
Andenes		
Ka-SACR and W-SACR (matched footprint co-scanning radars)	35- and 95-GHz reflectivity ( $Z_e$ ), Doppler velocity and spectra	Dual wavelength ratio and cloud and precipitation properties
KAZR (profiling)	35-GHz reflectivity, Doppler velocity, and spectra	Hydrometeor fall speed and air vertical velocity
AERI (Atmospheric Emitted Radiance Interferometer)	Downwelling radiance from atmosphere	Temperature and humidity profiles
MWR 2C and 3C (microwave radiometer)	Brightness temperature at 23.8 and 31.4 GHz	Column integrated liquid water and water vapor
MPL (micropulse lidar)	Backscatter power and polarization	Cloud base height, cloud optical depth, dust layers
CEIL (ceilometer)	Backscatter power	Cloud base height, PBL height
TSI (total sky imager)	Direct and indirect solar radiation	Cloud fraction
LDIS (laser disdrometer)	Fall speed and size of hydrometeor particles	Precipitation rate and size distribution, derived $Z_e$
MET (meteorology)	WXT530 weather station	Sea level pressure, surface temperature, humidity, and wind, precipitation rate
RWP (wind profiler)	1,290-MHz reflectivity and Doppler velocity	Wind profiles
ECOR (eddy correlation)	High-frequency humidity, temperature, and 3D momentum	Surface latent heat, sensible heat, and momentum fluxes
AOS (Aerosol Observing System)	See supplement	Aerosol sizing and chemistry, gas chemistry
MFRSR (Multi-Filter Rotating Shadowband Radiometer)	Diffuse and direct irradiance between 360 and 1,070 nm	Diffuse and direct radiation in the visible and near-infrared
Skyrad (radiometer)	Downwelling broadband shortwave and longwave irradiance	Cloud fraction
Radiosondes (6-hourly)	Temperature, pressure, humidity, wind profiles	Stability, integrated water vapor, etc.
Bear Island		
MRR (Univ. Cologne)	Rain rate, 24-GHz reflectivity, Doppler velocity	Snowfall rate
MWR (microwave radiometer)	Brightness temperature at 23.8 and 31.4 GHz	Column integrated liquid water and water vapor
MPL + CEIL	Backscatter power and polarization	Cloud base height, cloud optical depth, PBL height, dust layers
TSI (total sky imager)	Direct and indirect solar radiation	Cloud fraction
LDIS (laser disdrometer)	Fall speed and size of hydrometeor particles	Precipitation rate and size distribution, derived $Z_e$
MET (meteorology)	WXT530 weather station	Surface meteorology, precipitation rate
DL (Doppler lidar)	Backscatter power, doppler velocity	BL wind profiles
ECOR	High-frequency humidity, temperature, and 3D momentum	Surface fluxes
CEIL (ceilometer)	Backscatter power	Cloud base height, PBL height, clear-sky optical depth
Radiosondes (3-hourly during CAOs)	Temperature, pressure, humidity, wind profiles	Stability, integrated water vapor, etc.

At Bear Island, CAO conditions were more common (38 days in total during COMBLE) and more intense (average  $M$  value of 4.5 K)(Fig. 4a) than along the northern Scandinavian coast, consistent with the climatology. However, BL convection was suppressed between ~1 and 20

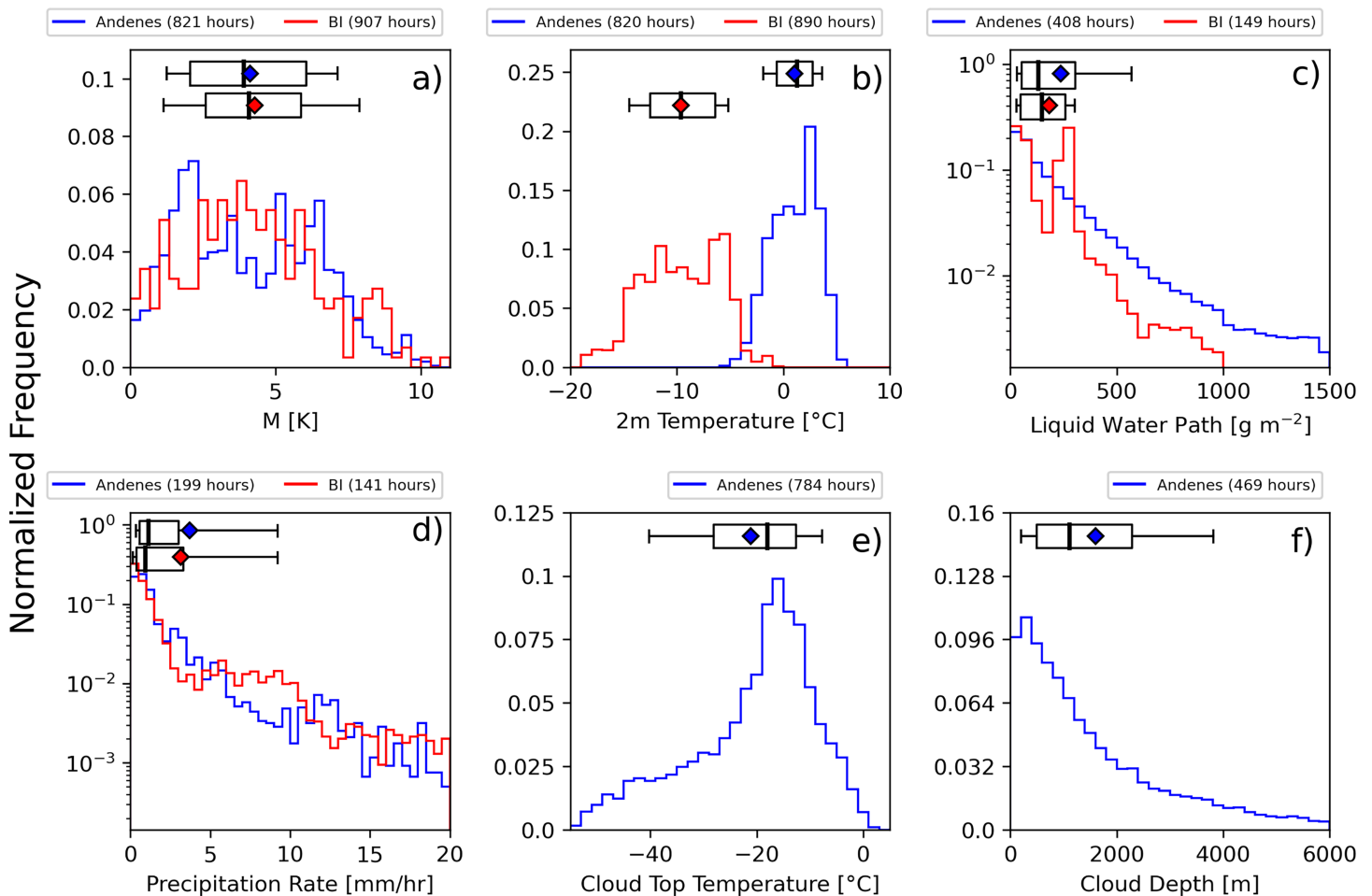


Fig. 4. Histograms of (a)  $M$  values, (b) surface temperature, (c) cloud LWP, (d) precipitation rate, (e) cloud-top temperatures, and (f) cloud depth, during all CAOs at Andenes (blue) and at Bear Island (BI, red) during COMBLE. Also shown are the 10th, 30th, 50th (median), 70th, and 90th percentiles (box with whiskers), plus the mean (blue/red diamond). Cloud-top temperature and cloud depth data are not available for Bear Island.

March 2020 when the marginal ice zone extended south from eastern Svalbard toward Bear Island, resulting in very low surface temperatures during CAOs on the island (see supplement). Cloud vertical structure information at Bear Island was limited: the only profiling radar during COMBLE, the University of Cologne MicroRain Radar (MRR), was range-limited to 1.0 km above ground level. Profiling radar data and satellite imagery (as in Fig. 1) indicate that Bear Island CAO clouds generally were shallow (<1.0 km) and aligned in cloud streets, whereas the CAO clouds near Andenes were deeper and usually assumed an open cellular arrangement. A summary of all CAO episodes and their characteristics at both locations is given in the “Objectively defined cold-air outbreaks during COMBLE” section in the online supplemental material.

Radar echoes were often rather strong during CAOs at Andenes, with a mean low-level reflectivity of  $\sim 12$  dBZ, extending to ground level (Fig. 5a). (At the time of writing, the KAZR reflectivity calibration was not final, and published values are believed to be 4–5 dBZ too low, as detailed in the supplement.) The mean hydrometeor vertical velocity, which is a proxy for reflectivity-weighted mean fall speed, was rather small in magnitude ( $\sim -1.0$  m s<sup>-1</sup>, Fig. 5b). This high reflectivity and low fall speed near the surface indicate that precipitation fell as snow, with little riming on average. Heavily rimed particles (graupel) were observed on occasion, as inferred from disdrometer data. Some 12% of the profiles experienced hydrometeor lofting (Fig. 5b), and these typically were associated with a higher Doppler spectral width (Fig. 5c), indicating turbulence and/or fall speed diversity.



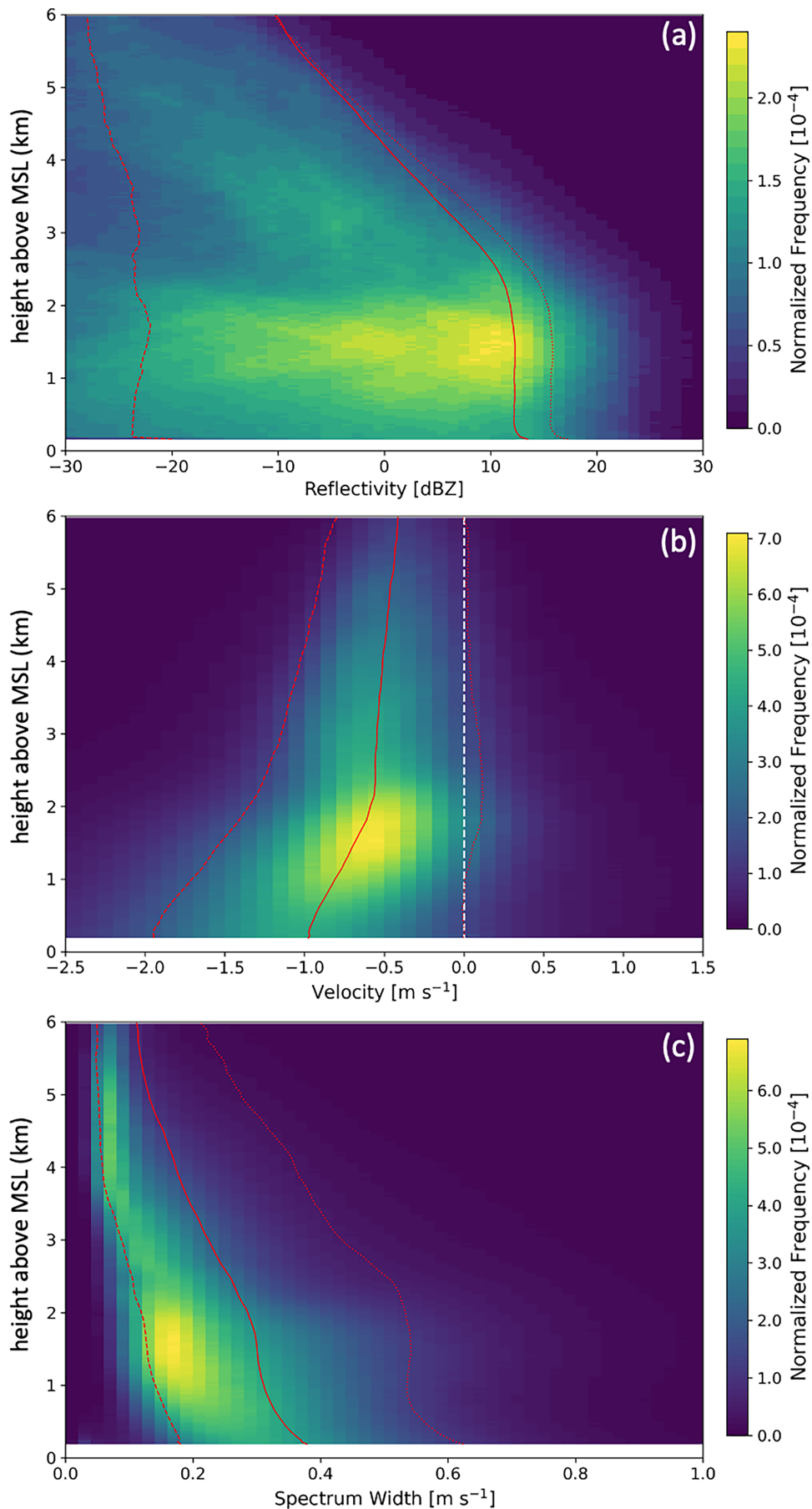
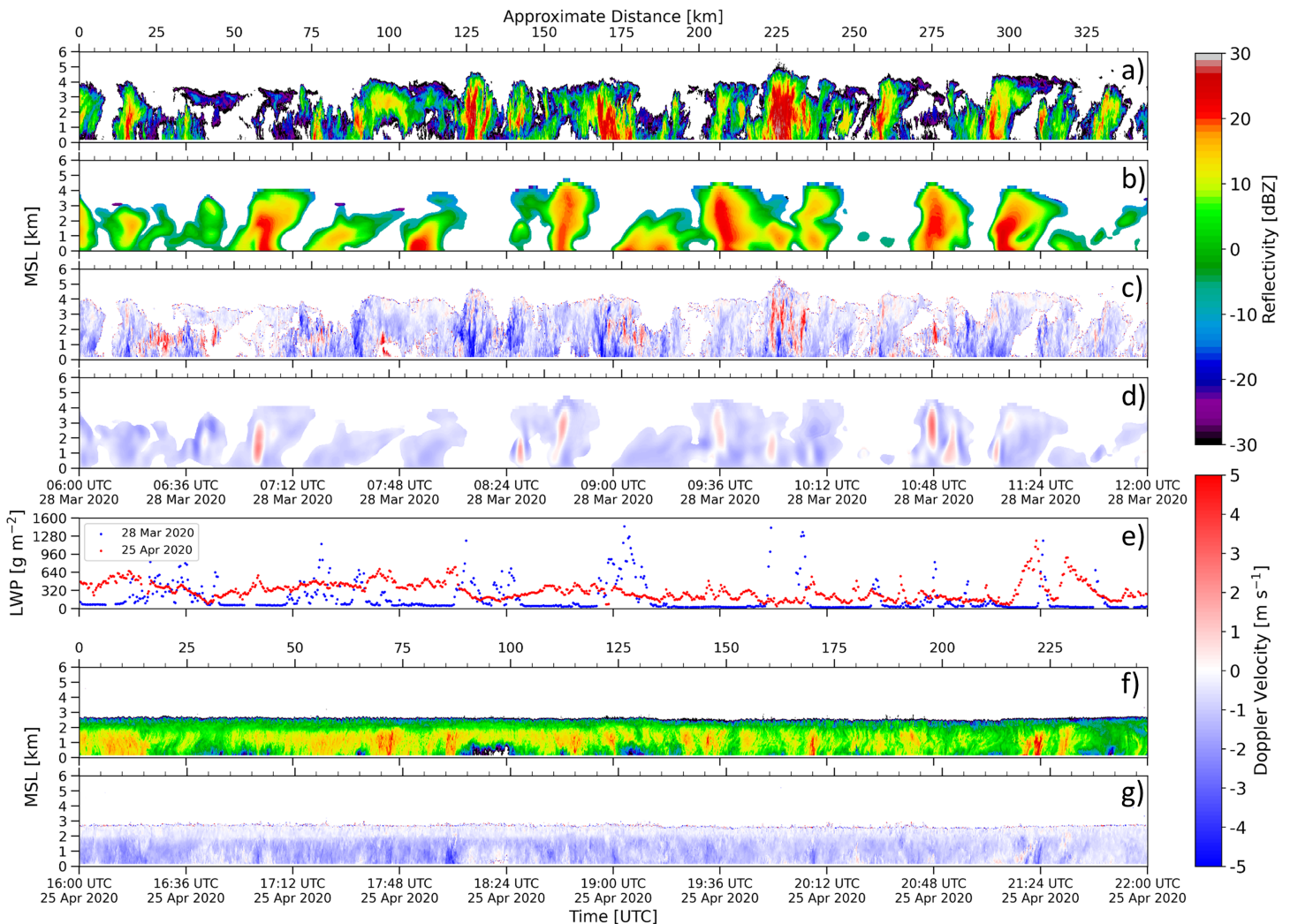


Fig. 5. Frequency by altitude display of KAZR (a) reflectivity, (b) Doppler velocity, and (c) spectral width at Andenes, during all CAO periods. From left to right, the red lines are the 10th percentile, the mean, and the 90th percentile.

The spectrum of CAO cloud properties is rather continuous (Figs. 4 and 5), but two cloud modes can be distinguished, depending on environmental conditions. Mode A, defined by high  $M$  values and/or strong surface winds, is characterized by pockets of strong updrafts and convective turbulence (alternating with decaying convective cells), occasionally high reflectivity with heavy surface precipitation rate, high cloud tops (with a secondary peak around 3.5 km MSL), rather low LWP on average, and broken cloud cover. Yet mode B, defined by low  $M$  values and/or weak surface winds, typically is associated with weak vertical drafts (up- and downdrafts) and turbulence, cloud tops around 2 km MSL, widespread but low reflectivity values, light precipitation rate, nearly overcast cloud cover, rather high amounts of supercooled liquid water, and common presence of cloud-top generating cells. Contrasts of this type are being explored further.

An example of the more intense CAO mode A is shown in Figs. 6a and 6c, depicting a sequence of convective cells and their (hydrometeor) vertical motions. During this 6-h period on 28 March, the average  $M$  value was 6.9 K, the surface wind speed was  $13.1 \text{ m s}^{-1}$ , and the SST-based CAPE was  $1,186 \text{ J kg}^{-1}$  at the AMF1 site. In contrast, the mode B cloud regime example shown in Figs. 6f and 6g (25 April) has an average  $M$  value of 0.9 K, a wind speed of  $9.1 \text{ m s}^{-1}$ , and an SST-based CAPE of  $112 \text{ J kg}^{-1}$ .



**Fig. 6.** Time–height transect of radar reflectivity from (a) KAZR and (b) model, and hydrometeor vertical velocity from (c) KAZR and (d) model, for the 28 Mar 2020 case, an example of mode A cloud structure. The model output calculations assume Ka-band scattering. The distance scale on top is based on the average wind speed between the surface and 5 km over the time of the transect. (e) Liquid water path (LWP) from radiometer for the same time period (blue), and for a mode B example, on 25 Apr (red). (f) KAZR reflectivity and (g) KAZR hydrometeor vertical velocity for this mode B example.

**Measurements of ice nucleating particles and other aerosol particles.** The Aerosol Observing System (AOS) at Andenes collected data on size distributions and concentrations of cloud condensation nuclei (CCN) and ice nucleating particles (INPs), and compositions of INP (Table 1). Here, we focus on INPs, which were measured using filter collections, resuspension of particles into pure water, and assessment via immersion freezing analysis, as described in the supplement. This method, which follows previous measurement efforts with the Colorado State University ice spectrometer (e.g., McCluskey et al. 2018), has now been standardized for mentored use with the DOE ARM program. Immersion freezing INP concentrations for 16 filters collected during identified COMBLE CAO events (“Objectively defined cold-air outbreaks during COMBLE” section in the supplemental material) are shown in Fig. 7. These Arctic INP data are compared to analogous samples collected in the Southern Ocean during the Measurements of Aerosols, Radiation and Clouds over the Southern Ocean (MARCUS) campaign (McFarquhar et al. 2021). It is clear that the INP population concentrations at this coastal site during CAOs are, on average, up to an order of magnitude higher than measured in the remote marine boundary layer over the Southern Ocean. This difference remains to be critically explored in future analyses as having a source from enhanced emissions of INPs in sea spray aerosol (SSA) particles or due to mixing of INPs of free tropospheric origin into the CAO marine boundary layer. Comparison to the SSA INP parameterization of McCluskey et al. (2018), fashioned around data collected at the Mace Head station in Ireland during summer conditions, is also shown in Fig. 7 (as M18).

To constrain M18 for COMBLE, we have applied the estimated upper bounds of total aerosol surface area derived from the COMBLE AOS dataset for CAO conditions. This parameterization, which has shown some success in describing Southern Ocean marine INP concentrations (McCluskey et al. 2018), cannot explain the nature of the INPs measured during the COMBLE CAOs at Andenes. We note that M18 does not include a description of enhanced marine organic INPs that have been found to be present in some North Atlantic and Arctic sea surface microlayers (Wilson et al. 2015), and found episodically in the North Atlantic summer atmosphere (McCluskey et al. 2018). Errors expected from the use of two common, generalized parameterizations for INPs applied in regional and global models become evident in Fig. 7. These are the default non-aerosol-aware parameterization used in

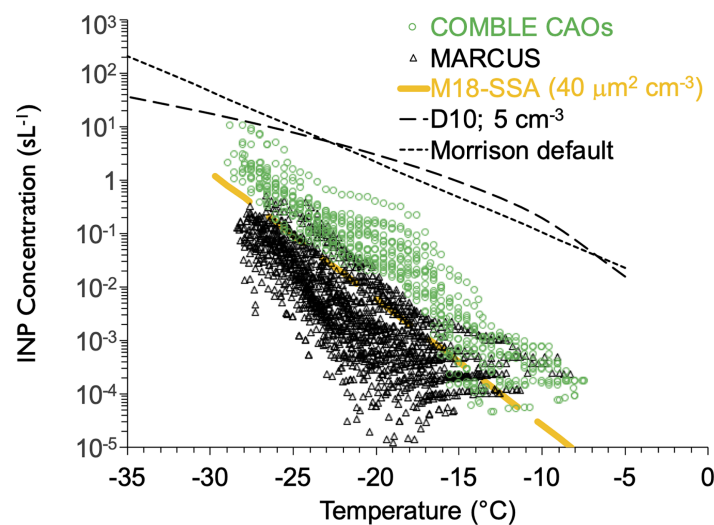


Fig. 7. INP concentrations vs temperature in 16 CAO events. Shown for contrast are data from Southern Ocean (MARCUS) studies. Also included are parameterized INP concentrations on the basis of the spectra used as default in the Morrison microphysics scheme (Morrison and Gettelman 2008), from DeMott et al. (2010; D10) using  $>0.5\text{-}\mu\text{m}$  aerosol concentrations for typical marine BL conditions at COMBLE, and for primary sea spray aerosol INPs on basis of the parameterization of McCluskey et al. (2018) (M18-SSA) at maximum CAO aerosol surface area conditions at COMBLE.

the Morrison microphysics scheme (Morrison and Gettelman 2008), and the “global” INP parameterization of DeMott et al. (2010), constrained using aerosol particle concentrations at sizes larger than  $0.5 \mu\text{m}$ . [DeMott et al. (2010) suggested that their parameterization may not be applicable to marine BL aerosol particles.] Explaining and properly parameterizing the sources of INPs feeding COMBLE storms during CAOs will require deeper inspection of datasets from COMBLE, MOSAiC, and elsewhere, and specialized investigations of the composition and sources of INP.

### **Case study: 28–29 March 2020**

The definition of a CAO as a sustained period of thermal instability and onshore flow [“Supplemental Bear Island (S2) site” section] yields 49 (39) CAOs at Andenes (Bear Island) during COMBLE, as detailed in the “Objectively defined cold-air outbreaks during COMBLE” section in the supplement. These events cover a broad range of upstream temperatures, stabilities, and wind speeds. Three of these were particularly intense and long lived: 2–6 February, 12–13 March, and 27–30 March 2020. All three episodes had periods of deep convection (4–5 km deep) with trajectories linking Andenes to the Arctic ice edge in the Fram Strait (Fig. 1). The 2–6 February case was the most persistent case; it featured a polar low passing north of Andenes, and both open and closed cells over the course of the event, with variable cloud tops. The 12–13 March case witnessed the highest  $M$  values, in the cold air behind a polar low; virtually all instruments collected good data in this case (see supplement).

Here, we illustrate the 27–30 March 2020 case (Fig. 1). This event had an average  $M$  value of 6.6 K, and a 2.5-day-long period of 4–5-km deep convection. We conducted a Weather Research and Forecasting (WRF) limited-area model (LAM) simulation of this case, driven by the ERA5 reanalysis. The outer and inner domains of this convection-permitting simulation are resolved by horizontal grid cell spacings of 3 and 1 km, respectively. We use a vertical grid cell spacing of  $\sim 50$  m from near the surface to 5 km AGL to better represent the fine-scale BL structure and entrainment across the BL top. The inner domain spans the distance between the ice edge in the Fram Strait and northern Norway. Additional information about this simulation can be found in Juliano et al. (2021).

Results from the simulations provide insight into the physical processes relevant to the CAO evolution that cannot be gleaned from the observations alone. At the beginning of the event, a mature polar low (or subsynoptic low) was located southeast of Svalbard and over the Barents Sea. Low-level cold air advection and strong northwesterly winds behind the low-pressure circulation supported intense surface heat fluxes, resulting in persistent CAO conditions at Andenes. Convective roll-like cloud structures initiated near the ice edge, widened with increasing fetch as the BL deepened, and eventually transitioned into cellular cloud structures (Fig. 1), a transition nicely captured in the simulation. By midday on 29 March, low-level winds weakened and cold-air advection mostly vanished; the cloud streets were not as strongly linked to the ice edge and more widely spaced cellular structures appeared near Andenes.

This LAM captures the depth, width, and spacing of the cellular convection at Andenes reasonably well (Fig. 6). A grid spacing around 1 km appears sufficient also to capture the HCRs and transverse bands in marine CAOs (e.g., Chechin et al. 2013; Campbell et al. 2018). To facilitate a direct comparison with the Ka-band radar data, we postprocessed the necessary WRF variables (including hydrometeor mixing ratios and number concentrations, and state variables) using the Cloud Resolving Model Radar Simulator (CR-SIM; Oue et al. 2020). The model’s performance at Andenes is an assessment of the accuracy in which the model captures relevant processes from the ice edge down to Andenes, a  $\sim 1,200$ -km distance. The 1-km grid cell spacing domain captures the resulting cloud depth and the rather uniform wind profile well (Fig. 8). The model agrees with radiosonde data that the SST-based convective available

potential energy (CAPE) just off the Norwegian coast is around  $1,000 \text{ J kg}^{-1}$ . The resulting convective up- and downdrafts significantly perturb the humidity and the temperature profiles at small scales, both in the model and according to the 3-hourly radiosonde data (not shown). Both soundings shown in Fig. 8 present in-cloud conditions, but significant drying occurs between the convective cells, at all levels (not shown). The lifting condensation level is high enough (Fig. 8) to allow significant convective cold pools to form. Therefore, it is more meaningful to compare distributions of convective parameters such as CAPE, an effort that is currently in progress.

The observed radar profiles show multiple cloud cells with cloud tops between 4 and 5 km MSL (Fig. 6a). Individual cells are in different stages of their development: some cells are characterized by high reflectivity in the upper cloud region, overshooting tops, strong updrafts, and high spectral widths, suggesting strong turbulence. Additionally, radiometer data indicate large LWP values (sometimes exceeding  $1,000 \text{ g m}^{-2}$ ) in those cells (Fig. 6e), and surface temperature measurements reveal no clear cold air anomaly. Thus, these cells are likely developing/maturing. In contrast, other cells in the same transect are in a decaying stage, as the highest reflectivity is found near the surface and the Doppler velocity is dominated by downward motion (Fig. 6c). These cells also have lower spectral widths, virtually no cloud liquid water, and a well-defined surface cold pool, indicative of precipitation (not shown). This suggests that convective cells experience a life cycle, which in turn may impact the cloud macroscale structure seen on satellite imagery.

The model also captures convective cells at different stages in their life cycle. Model output will be used to understand how cloud life cycle impacts new cell formation through cold pools, convergence, and low-level vorticity balance, and how these convective processes impact the overall open-cellular structure. At 1-km grid cell spacing, the model obviously fails to capture the fine updrafts and eddies evident in the KAZR Doppler velocity data (Figs. 6c,d), hence the interest in turbulence-resolving LES modeling.

### COMBLE-based modeling experiments

Several COMBLE-motivated modeling studies are currently in progress. These studies complement analysis of in situ and remote sensing measurements. Several well-documented CAO

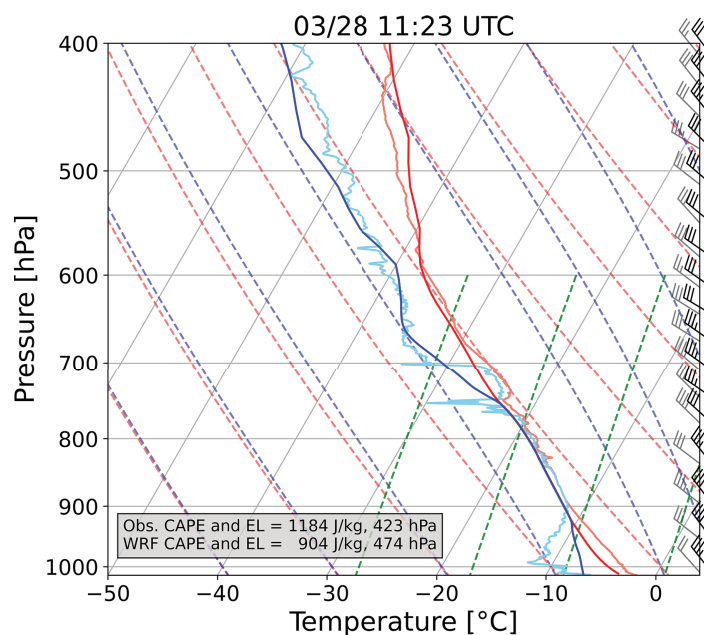


Fig. 8. Andenes skew  $T$  at 1123 UTC 28 Mar 2020 (radiosonde data, light blue, light red, and gray barbs) and corresponding WRF Model output (dark blue, dark red, and black barbs). The SST offshore from Andenes was about  $+6.1^\circ\text{C}$ ; the observed and simulated SST-based CAPE and equilibrium level (EL) are listed in the lower-left insert.

events, in particular, the three events listed in the “Case study: 28–29 March 2020” section, are expected to serve as test cases for detailed process-oriented modeling. Such case studies are important for assessing current understanding of complex surface–atmosphere interactions in the Arctic, and for evaluating model formulations. Especially the water cycle in CAOs, related to cloud formation and precipitation, has been shown to contribute to significant discrepancies between different model resolutions (Spensberger and Spengler 2021). Modeling is expected to make significant progress in the understanding and numerical representation of two related topics: the cloud macroscale structure and microphysical processes in mixed-phase clouds.

It has become a common practice to rely on well-evaluated, high-resolution models, both LAMs (as illustrated in the “Case study: 28–29 March 2020” section) and especially LES models, to serve as surrogate datasets for developing and testing parameterizations for climate models. This paradigm is being followed in COMBLE research. LES models resolve, rather than parameterize, exchanges in the BL, and capture cloud processes in the resolved eddies. They allow robust comparisons with the targeted observations collected in COMBLE and can take into account observational uncertainty. LES models are designed to capture the basic coupling of dynamical and microphysical processes at large-eddy scales and have been successfully used in previous observationally based Arctic case studies (e.g., Gryschka and Raasch 2005; Ovchinnikov et al. 2011; Fridlind and Ackerman 2018). Single column model (SCM) mode climate model simulations (e.g., Klein et al. 2009) are being run as well, to test climate model physics for a given set of boundary conditions and assumptions. Finally, a global, unconstrained, convection-permitting (3-km grid cell spacing) model is being examined in terms of CAO cloud properties and macroscale structure (Zheng et al. 2021).

Several previous ARM-sponsored field campaigns aimed at Arctic mixed-phase BL clouds have led to international model intercomparison projects (Klein et al. 2009; Morrison et al. 2011; Ovchinnikov et al. 2014). Such intercomparisons are invaluable in establishing confidence in LES results and characterizing their uncertainties. A similar intercomparison, but focusing on the dynamic “gray zone” regime of CAOs, was conducted by de Roode et al. (2019). In that study, the use of aircraft and quantitative satellite information was quite limited. A similar study, but with more in-depth observational guidance, is being planned, and will use one or more COMBLE case studies. Such a testbed provides a powerful tool for both evaluating and improving the ability of climate models to simulate the fundamental processes active in marine high-latitude CAOs. This intercomparison testbed will be used to evaluate new and existing parameterizations, in particular, their scale awareness, or the ability to appropriately rebalance relative contributions of processes at subgrid (parameterized) and resolved scales when the model resolution changes. A recent intercomparison conducted under the Global Atmospheric System Study (GASS), which tested the ability of LAMs with horizontal resolutions in the 1–16-km range to simulate an aircraft-sampled CAO event just north of Scotland (Field et al. 2017), can serve as a prototype for a COMBLE-based case. The planned modeling will draw on the experience from these activities, but will differ significantly in scientific focus and in the broader range of observations used to evaluate the simulations.

Two challenges exist in this endeavor, and they are rather unique to COMBLE. One is the vast distance between the ice edge and Andenes,  $O(1000)$  km, whereas LES must be conducted at a resolution that is at least four orders of magnitude smaller [ $O(0.1)$  km], to capture the bulk of the energy spectrum and relevant cloud processes. Therefore, the LES studies currently in progress assume a quasi-Lagrangian approach, whereby a relatively small domain, large enough to capture interacting convective cells (e.g.,  $50 \times 50$  km<sup>2</sup>), is advected with the prevailing BL wind. COMBLE provides the comprehensive measurements required to constrain a quasi-idealized Lagrangian CAO marine BL case study suitable for such side-by-side simulation with LES and climate models in SCM mode. Lagrangian CAO MBL budgets for coupled thermodynamic, aerosol (CCN and INP), and microphysical processes can be calculated

independently from observations and regional or climate model simulations, as well as LES and SCM simulations, providing a unified framework for understanding model performance and deficiency. One “hero” mesoscale to microscale coupled simulation is planned to capture the interactions among dynamics, thermodynamics, and microphysics across scales in one of the COMBLE CAO cases. The planned simulation includes an LES nest, consisting of approximately  $10,000 \times 3,000$  grid cells with grid spacing of 90 m, embedded in a parent mesoscale domain. Two additional LES nests, with grid spacing of 30 m, will be introduced into the first LES domain near the northern and the southern edges of the CAO.

The second challenge is that the upstream environment (the Arctic) is extremely data scarce, which makes model performance assessment at the level of individual case studies very challenging (Neggers et al. 2019). Model evaluation requires not just a critical assessment of model physics, but also (and first) a reverse engineering approach to correct biases in the driver datasets (that provide the upstream conditions) to match downstream conditions, i.e., the observations at Andenes or Bear Island. Separation between errors due to initial/boundary condition uncertainty and model physics uncertainty will be difficult. While there were eddy correlation probes on 10-m towers at both COMBLE sites, there were no in situ measurements of surface turbulent heat (and moisture) fluxes over the vast Norwegian Sea. The surface heat fluxes simulated by Lagrangian LES runs (with a fixed SST from the driver dataset, such as ERA5) may differ significantly from those in the driver dataset. A thorough evaluation of the sensitivity of the BL structure and cloud properties to surface fluxes should be of high priority in COMBLE and future studies. Radiosonde data and aerosol particle measurements were collected at Ny-Ålesund (Svalbard) and from the *Polarstern*, as part of the NASCENT and MOSAiC campaigns, respectively (Fig. 2). A preliminary backward trajectory analysis indicates that for brief periods in six CAOs, air sampled at Andenes can be traced back to the close vicinity of Ny-Ålesund or the *Polarstern*. In these cases, the observed thermodynamic profiles and aerosol information at either of these two sites can be used to drive simulations.

Ultimately, output from well-constrained LES in CAO environments will be used to evaluate global operational NWP models, as well as climate models. Special attention will go to the evaluation of key variables modulated by the CAO convective clouds. This includes the surface energy and momentum fluxes, which are enhanced by the convective and roll circulations that are subgrid scale in NWP and climate models; cloud-top height and BL depth, which are the result of a history of convective activity and cloud-top entrainment; and microphysical parameters (in particular, the aerosol budget, cloud liquid and ice water path, albedo, and precipitation rate), which depend both on surface exchange processes and BL depth. To evaluate the ability of climate models to simulate CAOs, hindcast simulations will be performed for the whole deployment period or a few selected convective episodes using frameworks such as the DOE’s Cloud-Associated Parameterization Testbed (Ma et al. 2015). This approach exposes the performance of parameterizations more clearly by mitigating the complicating effects of natural variability at synoptic, seasonal, and interannual time scales.

## Conclusions

During COMBLE between 1 December 2019 and 31 May 2020, the DOE ARM Mobile Facility and additional instruments were successfully deployed at a coastal site (Andenes) and an island site (Bear Island) along the ice-free Norwegian Sea, which climatologically is a global hotspot for CAOs over open water in winter and early spring. The Andenes site, on the northern Scandinavian coast, hosted multifrequency profiling and scanning radars, lidars, radiometers, and in situ aerosol, cloud, precipitation, trace gas, radiation, and flux measurements. Bear Island, located about halfway between northern Scandinavia and the Arctic ice, had a smaller instrument array, in particular, fewer remote sensors and aerosol probes.

The COMBLE campaign was conducted to examine the fetch-dependent relations between surface fluxes of heat and momentum, BL structure, aerosol, cloud and precipitation properties, and mesoscale circulations in marine CAOs. Accurate representation of the marine CAO regime in NWP and climate models is challenged by the subgrid-scale nature of the circulations, vertical exchanges, and cloud processes responsible for this cloud regime.

A cumulative total of 34 (38) days of CAO conditions at Andenes (Bear Island) during COMBLE, with a broad range of upstream temperatures, stabilities, and aerosol particle concentrations. Current observational analysis is focusing on three relatively persistent, intense outbreaks at Andenes, with convective cloud tops up to 4–5 km deep, but a broad spectrum of CAO conditions was observed in COMBLE, including many cases with cloud tops closer to 2 km MSL, typically with weaker convective drafts, much lighter precipitation, and yet higher cloud cover. The COMBLE dataset is being used as a modeling testbed to enhance understanding of mixed-phase cloud processes and cloud mesoscale organization, and to improve the representation of these processes in global models. A comprehensive suite of modeling activities is in progress, ranging from SCMs, LES, and LAMs to climate models. Plans are underway for a coordinated LES intercomparison effort, guided by a uniform driver dataset for at least one of the COMBLE case studies, and validated by COMBLE measurements and value-added products. This effort will be used to evaluate BL, aerosol, and cloud parameterizations in climate models.

**Acknowledgments.** The COMBLE campaign was enabled by an ARM Mobile Facility deployment proposal to the Office of Science of the U.S. Dept. of Energy. COMBLE research is possible through a number of DOE Atmospheric Systems Research (ASR) grants, including DE-SC0018927, DE-SC0021151, DE-SC0020171, DE-SC0021159, DE-SC0021116, DE-SC001862, and DE-SC0019251. This manuscript has been co-authored by employees of Brookhaven Science Associates, LLC, under Contract DE-SC0012704. The Pacific Northwest National Laboratory is operated by Battelle for the U.S. Dept. of Energy under Contract DE-AC05-76RL01830. Funding by the German Research Foundation (Deutsche Forschungsgemeinschaft, DFG) – Project-ID 268020496 – TRR 172 through the (AC)3 Transregional Collaborative Research Center is acknowledged. Special thanks to the Field Instrument Deployments and Operations team at the DOE Los Alamos National Lab for the successful deployment of the AMF1 and additional instruments in a challenging environment, and for the continued operation even after the onset of the coronavirus pandemic. Thanks also to the Norwegian Government’s Meteorological Service (Met Norway), under leadership of the Director of Observations Cecilie Stenersen, for supporting the DOE deployment effort in a variety of ways as mentioned in the text. And thanks to the many unnamed individuals in and around Andenes for assisting with COMBLE operations, sometimes in ways that were not anticipated. Finally, we appreciate the discussions with a number of scientists who already are using the COMBLE data, at ASR meetings, conferences, and workshops, including Ann Fridlind, Xue Zheng, Yunyan Zhang, and Steve Krueger.

**Data availability statement.** All COMBLE and auxiliary datasets are listed with DOIs in the supplemental material.



## Appendix: Abbreviations

AERI	Atmospheric emitted radiance interferometer
AMF	ARM Mobile Facility
ARM	Atmospheric Radiation Measurement
AOS	Aerosol Observing System
(M)BL	(Marine) boundary layer
<i>CALIPSO</i>	<i>Cloud-Aerosol Lidar and Infrared Pathfinder Satellite Observation</i>
CAO	Cold-air outbreak
CAPE	Convective available potential energy
CCN	Cloud condensation nuclei
CEIL	Ceilometer
COMBLE	Cold-Air Outbreaks in the Marine Boundary Layer Experiment
CR-SIM	Cloud Resolving Model Radar Simulator
DL	Doppler lidar
DOE	Department of Energy
ECMWF	European Centre for Medium-Range Weather Forecasts
EL	Equilibrium level
HCR	Horizontal convective roll
INP	Ice nucleating particles
KAZR	Ka-band profiling radar
LAM	Limited area model
LDIS	Laser disdrometer
LES	Large-eddy simulation
LWP	Liquid water path
MFRSR	Multi-Filter Rotating Shadowband Radiometer
MODIS	Moderate Resolution Imaging Spectroradiometer
MPL	Micropulse lidar
MRR	Micro Rain Radar
MSL	Mean sea level
MWR	Microwave radiometer
NWP	Numerical weather prediction
RWP	Radar wind profiler
SACR	Scanning cloud radar (Ka and W band)
SCM	Single column model
TSI	Total sky imager
VIIRS	Visible Infrared Imaging Radiometer Suite

## References

- Abel, S. J., and Coauthors, 2017: The role of precipitation in controlling the transition from stratocumulus to cumulus clouds in a Northern Hemisphere cold-air outbreak. *J. Atmos. Sci.*, **74**, 2293–2314, <https://doi.org/10.1175/JAS-D-16-0362.1>.
- Ahn, E., Y. Huang, S. T. Siems, and M. J. Manton, 2018: A comparison of cloud microphysical properties derived from MODIS and CALIPSO with in situ measurements over the wintertime Southern Ocean. *J. Geophys. Res. Atmos.*, **123**, 11 120–11 140, <https://doi.org/10.1029/2018JD028535>.
- Brümmer, B., 1999: Roll and cell convection in wintertime arctic cold-air outbreaks. *J. Atmos. Sci.*, **56**, 2613–2636, [https://doi.org/10.1175/1520-0469\(1999\)056<2613:RACCIW.2.0.CO;2](https://doi.org/10.1175/1520-0469(1999)056<2613:RACCIW.2.0.CO;2).
- Campbell, L. S., W. J. Steenburgh, Y. Yamada, M. Kawashima, and Y. Fujiyoshi, 2018: Influences of orography and coastal geometry on a transverse-mode sea-effect snowstorm over Hokkaido Island, Japan. *Mon. Wea. Rev.*, **146**, 2201–2220, <https://doi.org/10.1175/MWR-D-17-0286.1>.
- Chechin, D. G., C. Lüpkes, I. A. Repina, and V. M. Gryanik, 2013: Idealized dry quasi 2-D mesoscale simulations of cold-air outbreaks over the marginal sea ice zone with fine and coarse resolution. *J. Geophys. Res. Atmos.*, **118**, 8787–8813, <https://doi.org/10.1002/jgrd.50679>.
- DeMott, P. J., and Coauthors, 2010: Predicting global atmospheric ice nuclei distributions and their impacts on climate. *Proc. Natl. Acad. Sci. USA*, **107**, 11 217–11 222, <https://doi.org/10.1073/pnas.0910818107>.
- de Roode, S. R., and Coauthors, 2019: Turbulent transport in the gray zone: A large eddy model intercomparison study of the CONSTRAIN cold air outbreak case. *J. Adv. Model. Earth Syst.*, **11**, 597–623, <https://doi.org/10.1029/2018MS001443>.
- Dickson, R., J. Lazier, J. Meincke, P. Rhines, and J. Swift, 1996: Long-term coordinated changes in the convective activity of the North Atlantic. *Prog. Oceanogr.*, **38**, 241–295, [https://doi.org/10.1016/S0079-6611\(97\)00002-5](https://doi.org/10.1016/S0079-6611(97)00002-5).
- Field, P. R., R. J. Cotton, K. McBeath, A. P. Lock, S. Webster, and R. P. Allan, 2014: Improving a convection-permitting model simulation of a cold air outbreak. *Quart. J. Roy. Meteor. Soc.*, **140**, 124–138, <https://doi.org/10.1002/qj.2116>.
- , and Coauthors, 2017: Exploring the convective grey zone with regional simulations of a cold air outbreak. *Quart. J. Roy. Meteor. Soc.*, **143**, 2537–2555, <https://doi.org/10.1002/qj.3105>.
- Fletcher, J. K., S. Mason, and C. Jakob, 2016: A climatology of clouds in marine cold air outbreaks in both hemispheres. *J. Climate*, **29**, 6677–6692, <https://doi.org/10.1175/JCLI-D-15-0783.1>.
- Frasconi, A., and Coauthors, 2018: Building the next generation of climate modelers: Scale-aware physics parameterization and the “grey zone” challenge. *Bull. Amer. Meteor. Soc.*, **99**, E5185–E5189, <https://doi.org/10.1175/BAMS-D-18-0145.1>.
- Fridlind, A., and A. Ackerman, 2018: Simulations of Arctic mixed-phase boundary layer clouds: Advances in understanding and outstanding questions. *Mixed-Phase Clouds: Observations and Modeling*, C. Andronache, Ed., Elsevier, 153–183, <https://doi.org/10.1016/B978-0-12-810549-8.00007-6>.
- Gryschka, M., and S. Raasch, 2005: Roll convection during a cold air outbreak: A large eddy simulation with stationary model domain. *Geophys. Res. Lett.*, **32**, L14805, <https://doi.org/10.1029/2005GL022872>.
- IPCC, 2021: *Climate Change 2021: The Physical Science Basis*. V. Masson-Delmotte et al., Eds., Cambridge University Press, 3949 pp., [www.ipcc.ch/report/sixth-assessment-report-working-group-i/](http://www.ipcc.ch/report/sixth-assessment-report-working-group-i/).
- Juliano, T. W., B. Kosovic, L. Xue, B. Geerts, C. P. Lackner, M. Ovchinnikov, P. Wu, and Y. Wang, 2021: Modeled boundary layer and cloud properties observed during the 28–29 March 2020 Cold-Air Outbreaks in the Marine Boundary Layer Experiment (COMBLE) event. *2021 Fall Meeting*, New Orleans, LA, Amer. Geophys. Union, A45B–1833, <https://agu.confex.com/agu/fm21/meetingapp.cgi/Paper/980722>.
- Klein, S. A., and Coauthors, 2009: Intercomparison of model simulations of mixed-phase clouds observed during the ARM Mixed-Phase Arctic Cloud Experiment. I: Single-layer cloud. *Quart. J. Roy. Meteor. Soc.*, **135**, 979–1002, <https://doi.org/10.1002/qj.416>.
- Ma, H.-Y., and Coauthors, 2015: An improved hindcast approach for evaluation and diagnosis of physical processes in global climate models. *J. Adv. Model. Earth Syst.*, **7**, 1810–1827, <https://doi.org/10.1002/2015MS000490>.
- Marchant, B., S. Platnick, K. Meyer, and G. Wind, 2020: Evaluation of the MODIS Collection 6 multilayer cloud detection algorithm through comparisons with CloudSat Cloud Profiling Radar and CALIPSO CALIOP products. *Atmos. Meas. Tech.*, **13**, 3263–3275, <https://doi.org/10.5194/amt-13-3263-2020>.
- Mather, J. H., and J. W. Voyles, 2013: The ARM climate research facility: A review of structure and capabilities. *Bull. Amer. Meteor. Soc.*, **94**, 377–392, <https://doi.org/10.1175/BAMS-D-11-00218.1>.
- McCluskey, C. S., and Coauthors, 2018: A mesocosm double feature: Insights into the chemical makeup of marine ice nucleating particles. *J. Atmos. Sci.*, **75**, 2405–2423, <https://doi.org/10.1175/JAS-D-17-0155.1>.
- McCoy, D. T., D. L. Hartmann, and D. P. Grosvenor, 2014: Observed southern ocean cloud properties and shortwave reflection. Part II: Phase changes and low cloud feedback. *J. Climate*, **27**, 8858–8868, <https://doi.org/10.1175/JCLI-D-14-00288.1>.
- McCoy, I. L., R. Wood, and J. K. Fletcher, 2017: Identifying meteorological controls on open and closed mesoscale cellular convection associated with marine cold air outbreaks. *J. Geophys. Res. Atmos.*, **122**, 11 678–11 702, <https://doi.org/10.1002/2017JD027031>.
- McFarquhar, G. M., and Coauthors, 2021: Unique observations of clouds, aerosols and precipitation over the Southern Ocean: An overview of CAPRICORN, MARCUS, MICRE and SOCRATES. *Bull. Amer. Meteor. Soc.*, **104**, E894–E928, <https://doi.org/10.1175/BAMS-D-20-0132.1>.
- Miller, M. A., Nitschke, K., Ackerman, T. P., Ferrell, W. R., Hickmon, N., and Ivey, M., 2016: The ARM Mobile Facilities. *The Atmospheric Radiation Measurement (ARM) Program: The First 20 Years*, Meteor. Monogr., No. 57, Amer. Meteor. Soc., <https://doi.org/10.1175/AMSMONOGRAPHS-D-15-0051.1>.
- Morrison, H., and A. Gettelman, 2008: A new two-moment bulk stratiform cloud microphysics scheme in the Community Atmosphere Model, version 3 (CAM3). Part I: Description and numerical tests. *J. Climate*, **21**, 3642–3659, <https://doi.org/10.1175/2008JCLI2105.1>.
- , and Coauthors, 2011: Intercomparison of cloud model simulations of Arctic mixed-phase boundary layer clouds observed during SHEBA/FIRE-ACE. *J. Adv. Model. Earth Syst.*, **3**, M06003, <https://doi.org/10.1029/2011MS000066>.
- Naud, C. M., J. F. Booth, J. Jeyaratnam, L. J. Donner, C. J. Seman, M. Zhao, H. Guo, and Y. Ming, 2019: Extratropical cyclone clouds in the GFDL climate model: Diagnosing biases and the associated causes. *J. Climate*, **32**, 6685–6701, <https://doi.org/10.1175/JCLI-D-19-0421.1>.
- Neggers, R. A. J., J. Chylik, U. Egerer, H. Griesche, V. Schemann, P. Seifert, H. Siebert, and A. Macke, 2019: Local and remote controls on Arctic mixed-layer evolution. *J. Adv. Model. Earth Syst.*, **11**, 2214–2237, <https://doi.org/10.1029/2019MS001671>.
- Oue, M., A. Tatarevic, P. Kollias, D. Wang, K. Yu, and A. M. Vogelmann, 2020: The Cloud-resolving model Radar SIMulator (CR-SIM) version 3.3: Description and applications of a virtual observatory. *Geosci. Model Dev.*, **13**, 1975–1998, <https://doi.org/10.5194/gmd-13-1975-2020>.
- Ovchinnikov, M., A. Korolev, and J. Fan, 2011: Effects of ice number concentration on dynamics of a shallow mixed-phase stratiform cloud. *J. Geophys. Res.*, **116**, D00T06, <https://doi.org/10.1029/2011JD015888>.
- , and Coauthors, 2014: Intercomparison of large-eddy simulations of Arctic mixed-phase clouds: Importance of ice size distribution assumptions. *J. Adv. Model. Earth Syst.*, **6**, 223–248, <https://doi.org/10.1002/2013MS000282>.
- Papritz, L., and T. Spengler, 2017: A Lagrangian climatology of wintertime cold air outbreaks in the Irminger and Nordic seas and their role in shaping air–sea heat fluxes. *J. Climate*, **30**, 2717–2737, <https://doi.org/10.1175/JCLI-D-16-0605.1>.
- , S. Pfahl, H. Sodemann, and H. Wernli, 2015: A climatology of cold air outbreaks and their impact on air–sea heat fluxes in the high-latitude South Pacific. *J. Climate*, **28**, 342–364, <https://doi.org/10.1175/JCLI-D-14-00482.1>.

- Pithan, F., and T. Mauritsen, 2014: Arctic amplification dominated by temperature feedbacks in contemporary climate models. *Nat. Geosci.*, **7**, 181–184, <https://doi.org/10.1038/ngeo2071>.
- , and Coauthors, 2018: Role of air-mass transformations in exchange between the Arctic and mid-latitudes. *Nat. Geosci.*, **11**, 805–812, <https://doi.org/10.1038/s41561-018-0234-1>.
- Saltikoff, E., M. Kurri, H. Leijnse, S. Barbosa, and K. Stiansen, 2017: Maintenance keeps radars running. *Bull. Amer. Meteor. Soc.*, **98**, 1833–1840, <https://doi.org/10.1175/BAMS-D-16-0095.1>.
- Shupe, M. D., and Coauthors, 2022: Overview of the MOSAiC expedition—Atmosphere. *Elementa*, **10**, 00060, <https://doi.org/10.1525/elementa.2021.00060>.
- Spensberger, C., and T. Spengler, 2021: Sensitivity of air-sea heat exchange in cold-air outbreaks to model resolution and sea-ice distribution. *J. Geophys. Res. Atmos.*, **126**, e2020JD033610, <https://doi.org/10.1029/2020JD033610>.
- Tornow, F., A. S. Ackerman, and A. M. Fridlind, 2021: Preconditioning of overcast-to-broken cloud transitions by riming in marine cold air outbreaks. *Atmos. Chem. Phys.*, **21**, 12 049–12 067, <https://doi.org/10.5194/acp-21-12049-2021>.
- Vavrus, S., 2004: The impact of cloud feedbacks on Arctic climate under greenhouse forcing. *J. Climate*, **17**, 603–615, [https://doi.org/10.1175/1520-0442\(2004\)017,0603:TIOCF0.2.0.CO;2](https://doi.org/10.1175/1520-0442(2004)017,0603:TIOCF0.2.0.CO;2).
- Wilson, T., and Coauthors, 2015: A marine biogenic source of atmospheric ice-nucleating particles. *Nature*, **525**, 234–238, <https://doi.org/10.1038/nature14986>.
- Young, G. S., D. A. R. Kristovich, M. R. Hjelmfelt, and R. C. Foster, 2002: Rolls, streets, waves, and more: A review of quasi-two-dimensional structures in the atmospheric boundary layer. *Bull. Amer. Meteor. Soc.*, **83**, 997–1001, [https://doi.org/10.1175/1520-0477\(2002\)083,0997:RSWAMA.2.3.CO;2](https://doi.org/10.1175/1520-0477(2002)083,0997:RSWAMA.2.3.CO;2).
- Zheng, X., Y. Zhang, S. A. Klein, C. Terai, B. Geerts, M. Deng, P. M. Caldwell, and B. Peter, 2021: The boundary layer and cloud field associated with marine cold air outbreaks (MCAOs) in the COMBLE observations and the SCREAM DYAMOND2 simulation. *2021 Fall Meeting*, New Orleans, LA, Amer. Geophys. Union, A45B–1830, <https://agu.confex.com/agu/fm21/meetingapp.cgi/Paper/956778>.